High Efficiency Fluorescent Electroluminescence with Extremely Low Efficiency Roll-Off Generated by a Donor–Bianthracene–Acceptor Structure: Utilizing Perpendicular Twisted Intramolecular Charge Transfer Excited State

Yue Yu, Lin Ma, Xiaolong Yang, Huixin Zhou, Hanlin Qin, Jiangluqi Song, Guijiang Zhou, Dongdong Wang, and Zhaoxin Wu**

Although phosphorescent and thermally activated delayed fluorescence (TADF) emitters can break through the spin statistics rules and achieve nearly 100% radiative exciton production (η_r), the swift efficiency roll-off as luminance increases due to the accumulation of lowest triplet excited states with relatively long lifetime is the fatal bottleneck for their lighting application. How to achieve high η_r and low efficiency roll-off simultaneously is still a challenge. To address this issue, two metal-free organic molecules are reported with a highly twisted donor–bianthracene–acceptor structure involving high-lying twisted intramolecular charge transfer (TICT) intermediate excited states, by which electroluminescent (EL) devices with both high η_r and extremely low efficiency roll-off could be realized. Significant low efficiency roll-off is achieved with about 99.1% of the maximum external quantum efficiency (EQE) maintained even at a high current density of 100 mA cm^{-2}, corresponding to luminance of 23615 cd m^{-2}, along with maximum EQE of 7.13% (η_r of 64.82%) in a doped green EL device with 9-(4-{10′-[4-(4,6-diphenyl-[1,3,5]triazin-2-yl)-phenyl]-[9,9′]-bianthracenyl-10-yl}-phenyl)-9H-carbazole as a host. The state-of-the-art low efficiency roll-off and enhanced η_r would be attributed to spin mixing of high-lying TICT singlet and triplet intermediate excited states, proving the great potential of such a host design strategy for their practical lighting application.

1. Introduction

Organic light-emitting diodes (OLEDs) are a promising alternative to traditional inorganic light-emitting diodes for the future lighting application due to their advantages,[1–7] and OLEDs have already been used in display from small- and medium-sized mobile devices to large TV screens. For practical lighting application, both high efficiency and low efficiency roll-off at high current density would be realized at the same time. It is well known that the recombination of the injected holes and electrons will form singlet and triplet excitons in a ratio of 1:3 controlled by spin statistics rules.[8] Due to spin-forbidden radiative transition from triplet exciton to ground state, only 25% of singlet excitons can be used to emit photons for conventionally used fluorescent emitting materials.[9] To achieve a nearly 100% internal quantum efficiency, we should make full use of both singlet and triplet excitons. By employing phosphorescent materials with heavy atom effect, entirely utilization of both singlet and triplet excitons can be realized due to enhancement of spin–orbit coupling,[10,11] and there are many reports on phosphorescent devices with unity internal quantum efficiency.[12–14] However, phosphorescent devices always exhibit serious efficiency roll-off at high current density caused by triplet–triplet annihilation (TTA) and triplet-polaron quenching originating from the accumulation of the long lifetime lowest triplet

Dr. Y. Yu, Dr. L. Ma, Prof. H. Zhou, Dr. H. Qin, Dr. J. Song
School of Physics and Optoelectronic Engineering
Xidian University
Xi'an 710071, P. R. China
Dr. Y. Yu, Dr. X. Yang, Prof. G. Zhou, Dr. D. Wang
Department of Chemistry
School of Science
Xi'an Jiaotong University
Xi'an 710049, P. R. China
E-mail: zhougj@mail.xjtu.edu.cn
The ORCID identification number(s) for the author(s) of this article can be found under https://doi.org/10.1002/adom.201800060.
Prof. Z. Wu
Key Laboratory of Photonics Technology for Information
Department of Electronic Science and Technology
School of Electronic and Information Engineering
Xi'an Jiaotong University
Xi'an 710049, P. R. China
E-mail: zhaoxinwu@mail.xjtu.edu.cn
Prof. Z. Wu
Collaborative Innovation Center of Extreme Optics
Shanxi University
Taiyuan 030006, P. R. China

DOI: 10.1002/adom.201800060

excited states,[15] and phosphorescent materials, which contain rare metals, for example, Ir, Pt, and Os, have high cost of commercial production. In order to get the low-cost and stable fluorescent materials with the full usage of both singlet and triplet excitons, the thermally activated delayed fluorescence (TADF) mechanism and the corresponding materials were reconsidered. In TADF molecule, lowest non-radiative triplet excited states (T_1) could be converted to lowest radiative singlet excited states (S_1) through reverse intersystem crossing (RISC) due to the small energy gap between the lowest excited state of singlet and triplet owing to effective separation of electron donor (D) and acceptor (A) by the donor–acceptor-type structure,[16–20] and charge transfer (CT) states become the lowest excited states, thus a nearly 100% η_r can be achieved. However, TADF-based devices do suffer from serious efficiency roll-off at high current density mainly because of TTA and singlet–triplet quenching caused by the accumulation of lowest triplet excited states with relatively long lifetime,[21,22] rendering them difficult to work under practical application condition. Recently Yang and Ma reported a series of fluorescent materials with hybridized local and charge-transfer (HLCT) emission.[23–26] By using moderate D and A groups and controlling the twisted angle to obtain appropriate electronic coupling between D and A, the intercross of CT and local excited (LE) states could be achieved. Singlet enhancement and efficiency roll-off reduction could be achieved through an RISC path between high-lying triplet and singlet states, reducing the accumulation of lowest triplet excited states. However, high-performance devices with high efficiency and low efficiency roll-off are still rarely reported,[23–26] the relatively high energy barrier during hot exciton RISC on account of moderate electronic coupling between D and A would impede the hot exciton RISC, thus leading to modest efficiency roll-off.

In this paper, we demonstrate a new strategy to achieve both high η_r of 64.82% and extremely low external quantum efficiency (EQE) roll-off of 0.9% from peak values to those even at a high current density of 100 mA cm^{-2} by spin mixing of high-lying perpendicular twisted intramolecular charge transfer (TICT) singlet and triplet excited states. We select 9,9′-bianthracene (BA) moiety as the central core, which have almost perpendicular electronic structure, TICT characteristics, and intense fluorescence emission of LE states, based on our investigation of fluorinated BA derivatives before,[27,28] and report two novel molecules with highly twisted D–BA–A structure by modifying BA with D and A on both sides, respectively. In the process of electron injection, high-lying TICT intermediate excited states with smaller singlet–triplet energy splitting due to the decreased electronic coupling between D and A by the almost perpendicular BA core would cause more efficient hot exciton RISC channel. An efficient singlet enhancement process occurred during high-lying TICT intermediate excited states reduces the occurrence of accumulation of T_1 excitons, which is confidently beneficial for the suppression of efficiency roll-off at high current density.

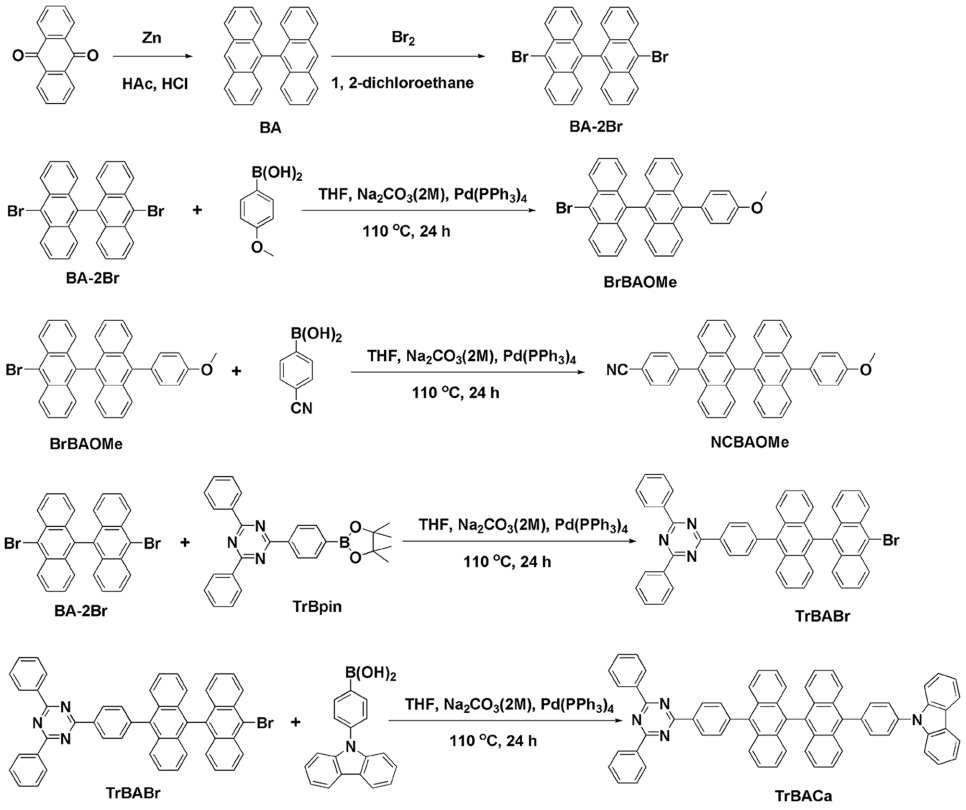

Scheme 1. Molecular structures and the synthetic routes of NCBAOMe and TrBACa.

2. Results and Discussion

2.1. Molecular Design, Synthesis, and Theoretical Computation

We use BA with TICT characteristics as the central core,[27–31] and add D or A on each side of BA core. Herein we introduce two D–BA–A structure molecules 4-[10′-(4-methoxyphenyl)-[9,9′]bianthracenyl-10-yl]-benzonitrile (NCBAOMe) and 9-(4-{10′-[4-(4,6-diphenyl-[1,3,5]triazin-2-yl)-phenyl]-[9,9′]bianthracenyl-10-yl}-phenyl)-9H-carbazole (TrBACa). For molecule NCBAOMe, the methoxyphenyl and benzonitrile act as the D and A, while for molecule TrBACa, the carbazole and triazin serve as the D and A, respectively. BA and 10,10′-dibromo-9,9′-bianthracene were synthesized according to the literature,[32,33] and then NCBAOMe and TrBACa were readily obtained via two sequential Suzuki couplings (see the Supporting Information); the molecular structures and the synthetic routes are outlined in **Scheme 1**. Both compounds were purified by temperature-gradient vacuum sublimation and fully characterized with ^{1}H NMR and element analysis.

The optimized geometry of the ground state (S_0) and excited state (S_1) was obtained using density functional theory (DFT) and time-dependent density functional theory (TD-DFT) methods with the functional CAM-B3LYP for NCBAOMe and TrBACa, respectively, and their structural details are shown in **Figure 1**a. For the optimized geometry of S_0, the dihedral angles (θ_2 and θ_6) between two adjacent anthracene moieties of NCBAOMe and TrBACa are nearly orthometric due to a steric repulsion of anthracene *peri*-hydrogen atoms (1,1′ and 8,8′-positions). From S_0 to S_1, the twist angle θ_2 of NCBAOMe and θ_6 of TrBACa are decreased to be 79°and 84°, respectively, while the twist angles θ_1 and θ_3 of NCBAOMe also exhibit a decreasing trend similar to the twist angles of θ_5 and θ_7 of TrBACa.

In order to examine the character of excited state, natural transition orbitals (NTOs) were calculated on the basis of

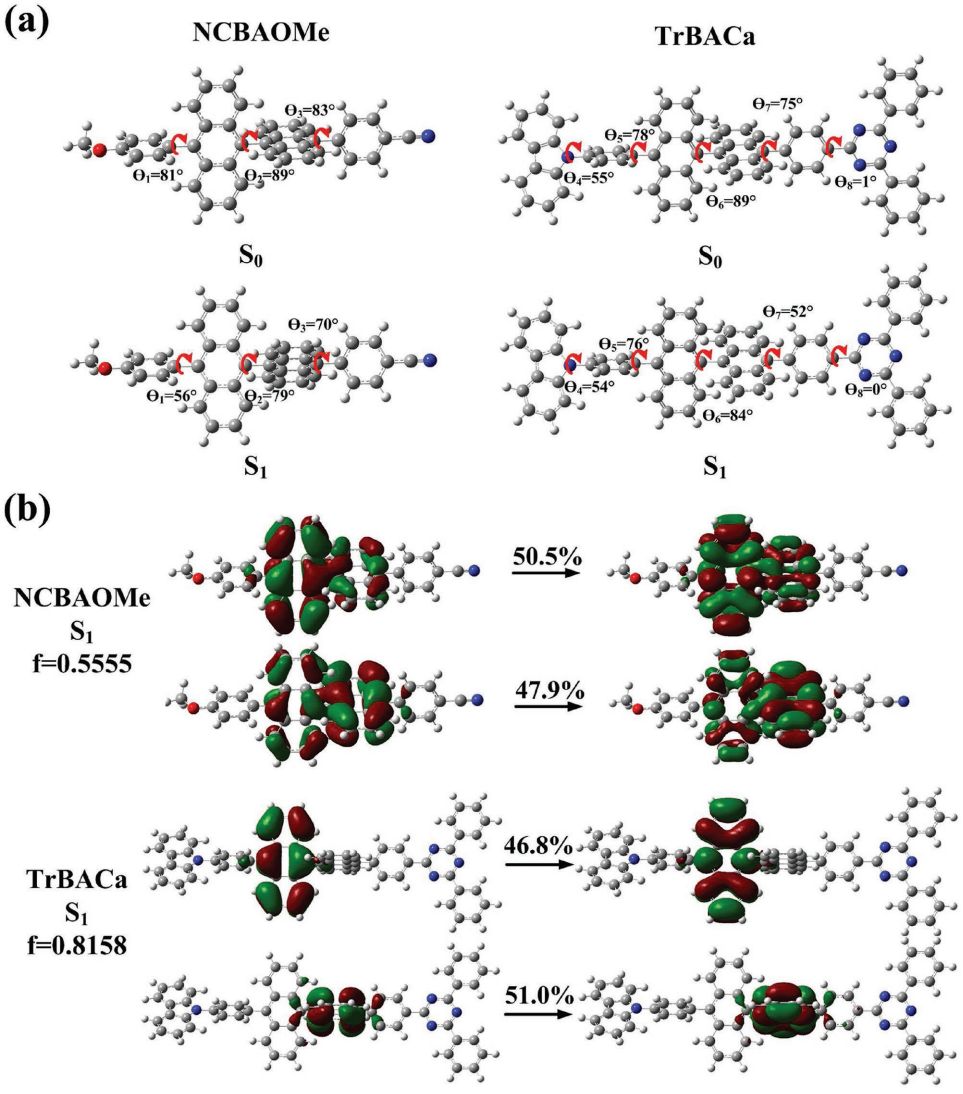

Figure 1. a) The optimized geometries of ground state S_0 and excited state S_1 of NCBAOMe and TrBACa. b)The dominant natural transition orbital pairs for the S_1 states of NCBAOMe and TrBACa calculating at the time-dependent TD-DFT/CAM-B3LYP level.

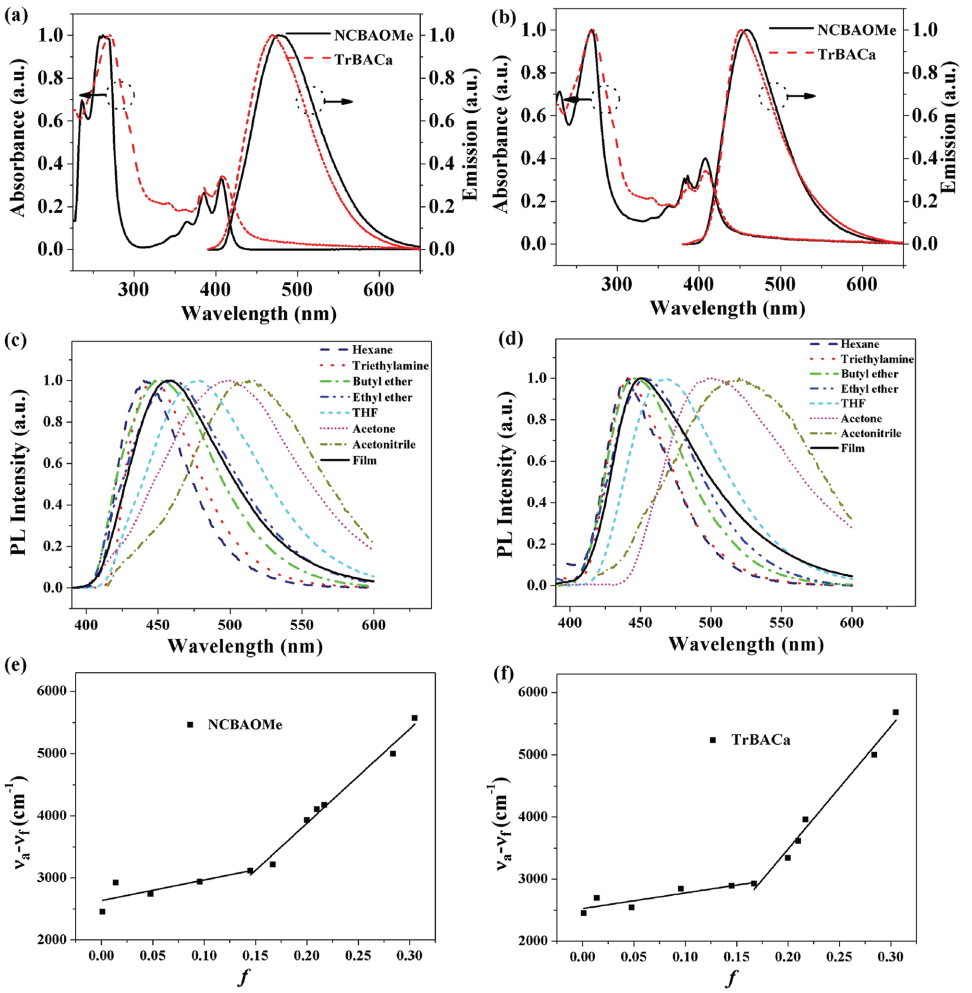

Figure 2. a) PL and absorption spectra of NCBAOMe and TrBACa in CH_2Cl_2. b) PL and absorption spectra of NCBAOMe and TrBACa in films. c) PL spectra of NCBAOMe in various solvents and in film. d) PL spectra of TrBACa in various solvents and in film. e) Linear correlation of orientation polarization ($f(\varepsilon, n)$) of solvent media with the Stokes shift ($\nu_a - \nu_f$) for NCBAOMe. f) Linear correlation of orientation polarization ($f(\varepsilon, n)$) of solvent media with the Stokes shift ($\nu_a - \nu_f$) for TrBACa.

TD-DFT/CAM-B3LYP/6-31G(d, p) level for S_1 states. As shown in Figure 1b, on the one hand, for the S_1 states of NCBAOMe and TrBACa, both "hole" and "particle" are populated on the BA central moiety with large overlap, thus the initial S_1 excited states of NCBAOMe and TrBACa display the mainly LE transition feature. On the other hand, the two pairs of NTOs for S_1 states of NCBAOMe are delocalized over the whole BA moiety compared with those of TrBACa, whose NTOs are localized on single anthracene part, indicating that the coupling of two anthracene units is enhanced and slight CT component may be formed in S_1 state for NCBAOMe due to the smaller twist angle between two adjacent anthracene moieties on the basis of optimized S_1 geometry obtained using DFT. The oscillator strength of NCBAOMe (0.5555) in S_1 state is lower than that of TrBACa (0.8158), which indicates that the higher radiative transition could be expected in TrBACa due to its strong LE character.

2.2. Photophysical and Excited State Properties

The normalized UV–vis absorption and photoluminescence (PL) spectra of NCBAOMe and TrBACa in dichloromethane (CH_2Cl_2) dilute solutions are shown in **Figure 2**a. Figure 2b shows these spectra in films (≈50 nm) obtained by thermal evaporation on a pre-cleaned quartz substrate. Their photophysical data are summarized in **Table 1**. NCBAOMe and TrBACa exhibit very similar absorption peaks in CH_2Cl_2 solutions, and absorption spectra of NCBAOMe and TrBACa in films are little redshifted relative to those in solutions. NCBAOMe and TrBACa in films show the common isolated characteristic vibronic structure at ≈342, 363, 384, and 406 nm due to the BA core. The PL emission peaks of NCBAOMe and TrBACa in films are observed at 457 and 451 nm, much blueshifted relative to those in CH_2Cl_2 solutions.

As shown in Figure 2c,d, when in different organic solvents with increase of the solvent polarity gradually from hexane to

Table 1. Physical properties of BAnFs.

Compound	λ_{max}^{Abs} a)/b) [nm]	λ_{max}^{PL} a)/b) [nm]	Φ_f c)	T_g/T_m d) [°C]	HOMO/LUMO^{exp} (E_g^{opt}) e) [eV]	HOMO/LUMO^{cal} ($\Delta E_{HOMO\text{-}LUMO}$) f) [eV]
NCBAOMe	263, 345, 364, 385, 402/267, 342, 363, 384, 406	483/457	0.68	176/487	−5.62/−2.75 (2.87)	−5.90/−1.96 (3.94)
TrBACa	270, 342, 363, 386, 402/270, 341, 362, 386, 406	478/451	0.89	193/512	−5.67/−2.77 (2.90)	−5.96/−1.98 (3.98)

a)Measured in CH_2Cl_2; b)Measured in solid thin film on quartz plates; c)Determined in CH_2Cl_2 using quinine sulfate (Φ_{PL} = 0.56 in 1.0 M H_2SO_4 solution) as standard; d)T_g: glass-transition temperature and T_m: melting point; e)The HOMO and LUMO energies were determined from cyclic voltammetry and the absorption onset in film; f)Values from DFT calculation.

acetonitrile, the PL emission peaks of NCBAOMe and TrBACa exhibit obvious solvatochromic effect with obvious redshifts of 77 and 81 nm, respectively, accompanied by broadened PL spectrum. This phenomenon is consistent with double fluorescence property of BA core. Apart from LE state, the fluorescence clearly occurs from a highly polar intramolecular CT state involving the TICT mechanism in polar fluid solvents.[29–31,34,35] In low-polarity solvents, upon the optical excitation, LE state with nearly orthogonal configuration, in which only one anthracene unit is excited to form the lowest singlet state, mainly contributes to luminescence. As the solvent polarity increases, BA core will undergo a symmetry breaking with formation of highly polar TICT state and the energy level of TICT state begins to degrade because of the interaction between the solvent field and the TICT state with large dipole moment, thus emission from TICT state can be observed after an apparent relaxation of torsion angle. In high-polarity solvents, TICT state with lowest energy level mainly contributes to fluorescence with large redshift. Moreover, we further estimated the dipole moments of S_1 state from the linear fitting analysis of the Stokes shift ($\nu_a - \nu_f$) and the solvent orientation polarizability ($f(\varepsilon, n)$), according to the Lippert–Mataga model (see the Supporting Information).[34] As shown in Figure 2e,f, NCBAOMe and TrBACa both show two-section lines with an inflection point, which indicates the existence of two different features of excited state. The dipole moment μ_e of NCBAOMe is calculated to be 12.6 D in low-polarity solvents and 20.1 D in high-polarity solvents. The value of 12.6 D could be attributed to the LE-dominating HLCT state revealing that the S_1 state still possessed obvious CT character, which is compliant with the NTO analysis in Figure 1b. The large dipole of 20.1 D should be considered as a CT-like state, which is close to the typical CT state molecule DMABN with a μ_e of 23 D.[36] TrBACa also displays two-section linear relations with μ_e of 8.4 D and 20.2 D, corresponding to LE-like state and CT-like state, respectively.

Figure 3 shows the fluorescence decay curves for emission of NCBAOMe and TrBACa in tetrahydrofuran (THF) dilute solution, the PL lifetimes of NCBAOMe and TrBACa were 11.79 and 3.42 ns, respectively, and the test results do not possess delayed component with long lifetime. In phosphorescence spectra measurement experiment of NCBAOMe and TrBACa in THF dilute solution at 77 K, no phosphorescence was observed, which indicated that T_1 excitons hardly formed due to the large energy gap between S_1 and T_1. We measured the photoluminescence quantum yields (η_{PL}s) of NCBAOMe and TrBACa in dilute CH_2Cl_2 solution using quinine sulfate as standard (η_{PL}= 0.56 in 1.0 M H_2SO_4 solution) to be 0.68 and 0.89. However, in solid film state, the η_{PL}s of NCBAOMe and TrBACa reduced to 0.23 and 0.29.

2.3. Thermal and Electrochemical Properties

Thermal properties were investigated by differential scanning calorimetry, and the resultant data are shown in Table 1. Both NCBAOMe and TrBACa exhibited good thermal stabilities. The glass-transition temperatures (T_gs) of NCBAOMe and TrBACa were determined to be 176 and 193 °C (Figure S1, Supporting Information), and NCBAOMe and TrBACa also exhibit high decomposition temperatures (corresponding to 5% weight loss) of 487 and 512 °C, demonstrating that these chromophores are suitable for vapor deposition in OLED fabrication due to the perpendicular-type configuration of their molecular structures. The highest occupied molecular orbital (HOMO) energy levels of NCBAOMe and TrBACa were measured to be −5.62 and −5.67 eV by cyclic voltammetric studies (Figure S2, Supporting Information). The cyclic voltammetric experiments were carried out in solutions of 0.1 M supporting electrolyte ([Bu_4N]ClO_4) and 1×10^{-3} M substrate in dry CH_2Cl_2 under a nitrogen atmosphere using ferrocene as an internal standard. The lowest unoccupied molecular orbital (LUMO) energy levels were calculated to be −2.75 and −2.77 eV, respectively, from their absorption edges of the optical absorption spectra.

2.4. Electroluminescent Properties

To investigate the carrier-transport properties of NCBAOMe and TrBACa, electron-only and hole-only devices with structure of [indium tin oxide (ITO)/LiF (1 nm)/1,3,5-tris(1-phenyl-1*H*-benzimidazol-2-yl)benzene (TPBi) (10 nm)/NCBAOMe or

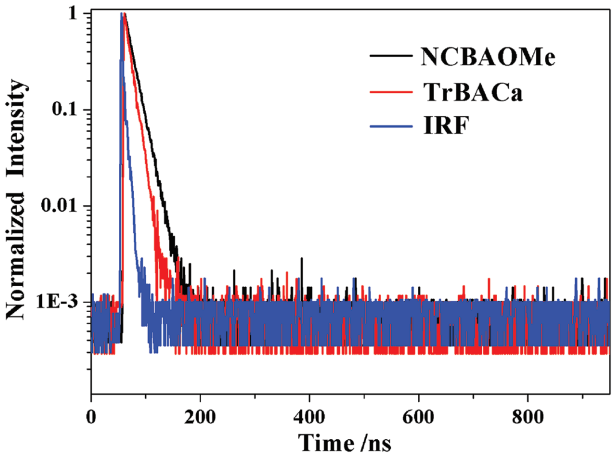

Figure 3. Photoluminescence decay curves of NCBAOMe and TrBACa in oxygen-free THF dilute solution excited at 379 nm.

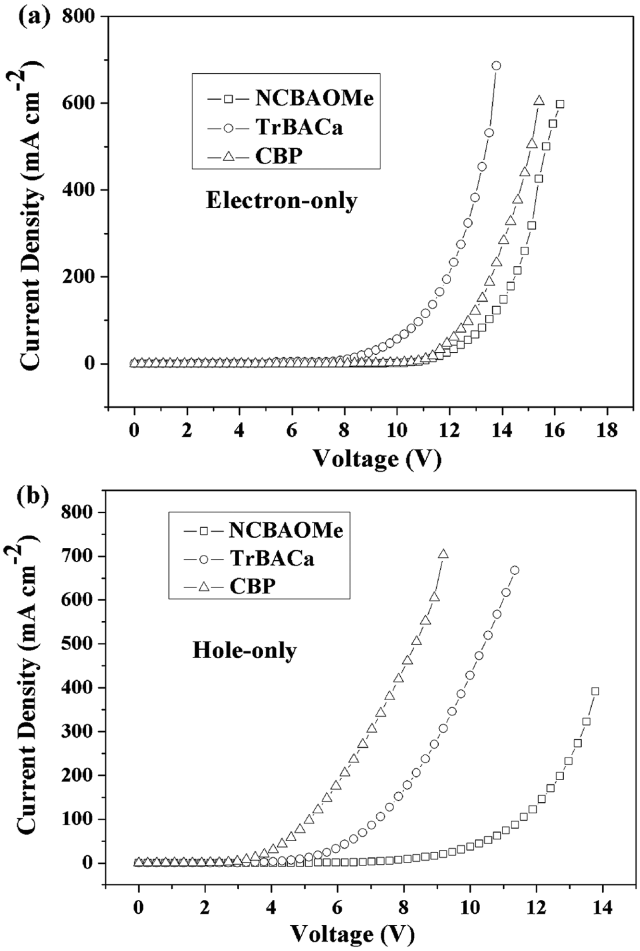

Figure 4. a) Current density–voltage characteristics for the electron-only devices consisting of ITO/LiF (1 nm)/TPBi (10 nm)/NCBAOMe or TrBACa (80 nm)/TPBi (10 nm)/LiF (1 nm)/Al (100 nm). b) Current density–voltage characteristics for the hole-only devices consisting of ITO/MoO_3 (3 nm)/NPB (10 nm)/NCBAOMe or TrBACa (80 nm)/NPB (10 nm)/MoO_3 (3 nm)/Al (100 nm).

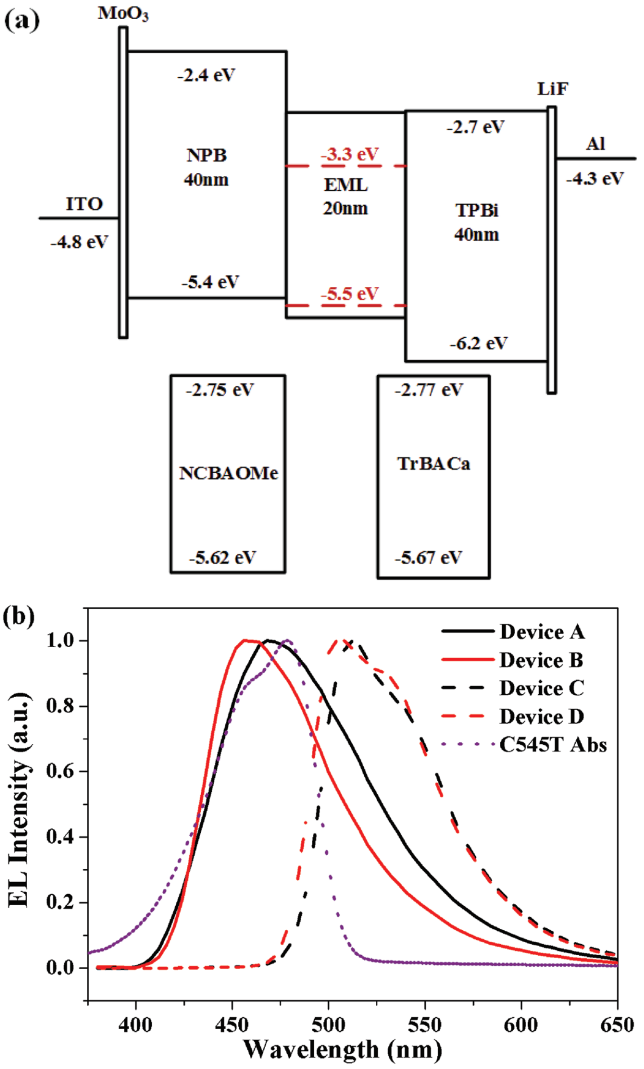

Figure 5. a) Device structure and the energy levels of main materials used in the device fabrication. b) Normalized EL spectra at 8 V and absorption spectra of C545T in film.

TrBACa or 4,4′-bis(*N*-carbazolyl)biphenyl (CBP) (80 nm)/TPBi (10 nm)/LiF (1 nm)/Al (100 nm)] and [ITO/molybdenum trioxide (MoO_3) (3 nm)/4,4′-bis[*N*-(1-naphthyl)-*N*-phenyl-amino] biphenyl (NPB) (10 nm)/NCBAOMe or TrBACa or CBP (80 nm)/NPB (10 nm)/MoO_3 (3 nm)/Al (100 nm)], respectively, were prepared. The well-known ambipolar conductive CBP was used as a comparison. As shown in **Figure 4**, at a given applied voltage, the current density of electron-only devices exhibits TrBACa > CBP > NCBAONe, and the current density of hole-only devices shows CBP > TrBACa > NCBAONe, suggesting their charge carrier mobility decreased in turn. As we all know, the hole mobility of CBP is higher than its electron mobility for an order of magnitude,[37] therefore, TrBACa are expected to have more balanced ambipolar conductive property.

We initially fabricated nondoped devices to examine the electroluminescent (EL) properties of NCBAOMe and TrBACa with the configuration [ITO/MoO_3 (3 nm)/NPB (40 nm)/NCBAOMe or TrBACa (20 nm)/TPBi (40 nm)/LiF (1 nm)/Al (100 nm)] (device A with NCBAOMe as emitting layer and device B with TrBACa as emitting layer). To investigate the EL performance of NCBAOMe and TrBACa as host materials, then doping devices have been constructed and evaluated by using the well-known 10-(2-benzothiazolyl)-1,1,7,7-tetramethyl-2,3,6,7-tetrahydro-1*H*,5*H*,11*H*-benzo[*l*]pyrano(6 7 8-*ij*)quinolizin-11-one (C545T) as the green fluorescent dopant. The device structures were [ITO/MoO_3 (3 nm)/NPB (40 nm)/NCBAOMe or TrBACa: C545T (20 nm)/TPBi (40 nm)/LiF (1 nm)/Al (100 nm)] (device C and device D), dopant C545T was doped in NCBAOMe or TrBACa to form the emitting layer with the optimal doping concentration of 1 wt%. In the above devices, MoO_3 was hole injection layer, NPB was utilized as hole transporting layer, TPBi was used as electron transporting layer and exciton blocking layer, and LiF as electron injection layer, respectively. **Figure 5**a shows the device structure and the energetics of main materials used in the device fabrication, good injection, and confinement of carrier charges in the emitting layer are achieved. Normalized EL spectra of these devices, along with absorption spectra of

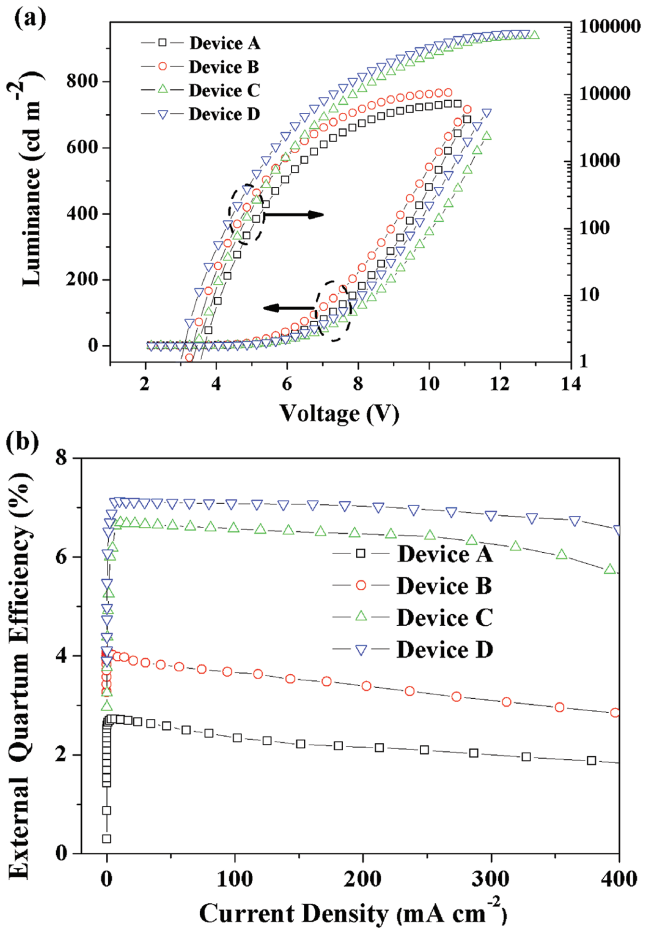

Figure 6. a) Current density–voltage–luminance characteristics of NCBAOMe and TrBACa devices. b) External quantum efficiency versus current density curves of NCBAOMe and TrBACa devices.

C545T in solid state, are shown in Figure 5b. Since the spectral overlap efficiency between EL spectra of host materials and absorption spectra of C545T, Förster energy transfer would efficiently occur. Both devices A and B exhibit blue emissions with Commission International de l'Éclairage (CIE) coordinates of (0.17, 0.22) and (0.16, 0.16). Compared to EL spectra of TrBACa, there is an obvious redshift in EL spectra of NCBAOMe due to greater probability of CT component according to the results of S_1 stat NTOs. The EL spectra of device C and D show green emissions of C545T, which are significantly different from EL emissions of nondoped devices.

The current density–voltage–luminance (*J*–*V*–*L*) characteristics and the EQE versus current density curves of these devices are illustrated in **Figure 6** and the key devices performances are listed in **Table 2**. For nondoped devices, the maximum luminance, maximum current efficiency, maximum power efficiency, and maximum EQE of device A are 7175 cd m^{-2}, 4.85 cd A^{-1}, 3.83 lm W^{-1}, and 2.72%, respectively. Furthermore, device B exhibited more excellent performances with a maximum luminance of 10 608 cd m^{-2}, a maximum current efficiency of 5.93 cd A^{-1}, a maximum power efficiency of 4.91 lm W^{-1}, and a maximum EQE of 4.09%. Assuming that light out coupling efficiency (η_{out}) is estimated as 20% for a glass substrate with an index of refraction n = 1.5,[38] charge balance factor (γ) is 100% in a properly designed device, and the η_{PL}s of NCBAOMe and TrBACa films are 0.23 and 0.29, we estimated η_rs of device A and device B to be 59.1% and 70.5% according to Equation EQE = $\eta_{out}\gamma\eta_r\eta_{PL}$, largely breaking through the limit of 25% in a conventional fluorescent device. It is worth noting that at a high current density of 100 mA cm^{-2} (corresponding to luminance of 4171 cd m^{-2} for device A and 5307 cd m^{-2} for device B), device A and device B exhibited slightly EQE roll-off of 14.0% and 10.5%, respectively, indicating that the η_r still kept above 50% of device A and device B. In this regard, NCBAOMe and TrBACa are more practical than TADF materials, which suffer from serious efficiency roll-off at high current density.[21,22] Compared to device A, device B with TrBACa as emitter showed lower EQE. This is mainly due to intense transition of LE state and more balanced ambipolar conductive property of TrBACa. The C545T-doped devices exhibited more excellent performance, the maximum luminance, maximum current efficiency, maximum power efficiency, and maximum EQE are 74 922 cd m^{-2}, 21.39 cd A^{-1}, 15.90 lm W^{-1}, and 6.69%, respectively, for device C and 82 235 cd m^{-2}, 23.83 cd A^{-1}, 19.19 lm W^{-1}, and 7.13%, respectively, for device D. We measured η_{PL}s of NCBAOMe: C545T (1 wt%) and TrBACa: C545T (1 wt%) films to be 0.63 and 0.55 using an integrating sphere, thus η_rs of device C and device D were estimated to be 53.10% and 64.82%. A distinctive merit is that the two doped devices exhibited desired stability, at a high current density of 100 mA cm^{-2} (corresponding to luminance of 20 919 cd m^{-2} for device C and 23 615 cd m^{-2} for device D), device C and device D exhibited negligible EQE roll-off of 2.2% and 0.9%, respectively. Even at a ultra high current density of 300 mA cm^{-2} (corresponding to luminance of 59 549 cd m^{-2} for device C and 68 702 cd m^{-2} for

Table 2. EL performance of NCBAOMe and TrBACa.

Device	EML	λ_{max}^{EL} [a)] [nm]	V_{on} [b)] [V]	L_{max} [c)] [cd m^{-2}]	η_{ext} [d)] [%]	η_c [d)] [cd A^{-1}]	η_p [d)] [lm W^{-1}]	EQE roll-off [e)] [%]	EQE roll-off [f)] [%]	CIE [a)] [x,y]
A	NCBAOMe	464	3.5	7175	2.72	4.85	3.83	14.0	26.5	(0.17,0.22)
B	TrBACa	452	3.2	10608	4.09	5.93	4.91	10.5	24.2	(0.16,0.16)
C	NCBAOMe:C545T	512	3.3	74922	6.69	21.39	15.90	2.2	7.2	(0.28,0.63)
D	TrBACa: C545T	508	3.0	82235	7.13	23.83	19.19	0.9	3.9	(0.27,0.61)

[a)]Values collected at 8 V; [b)]Turn-on voltage at 1 cd m^{-2}; [c)]Maximum luminance; [d)]Values collected at a peak efficiency; [e)]Values collected at a current density of 100 mA cm^{-2}; [f)]Values collected at a current density of 300 mA cm^{-2}.

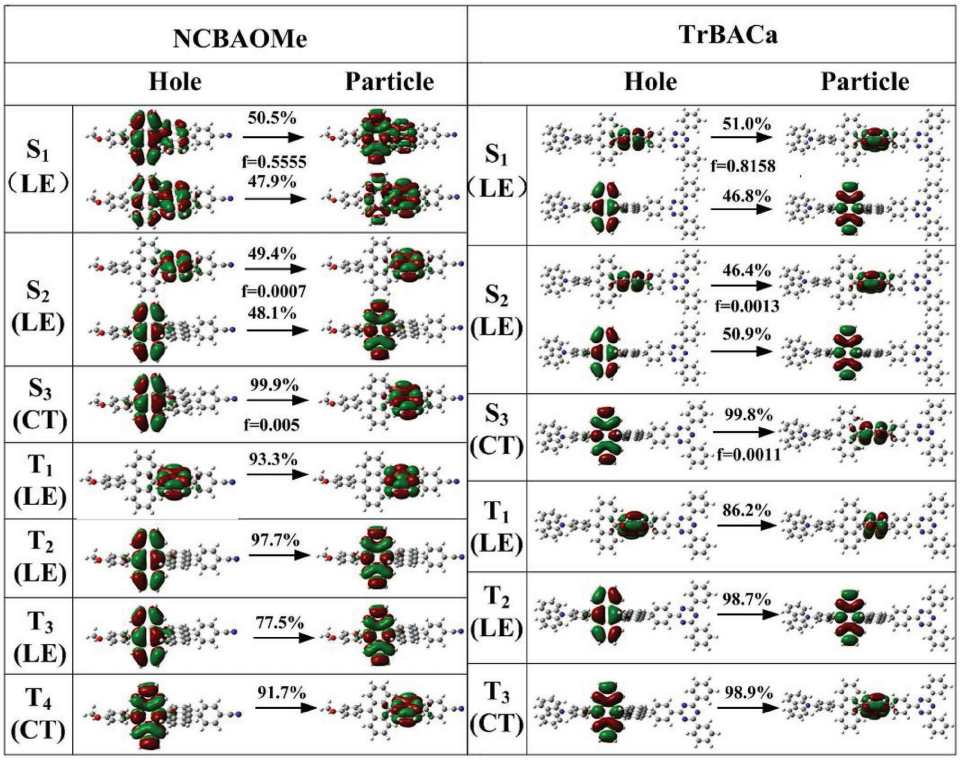

Figure 7. Natural transition orbitals (NTOs) of the first three or four singlet and triplet excited states for NCBAOMe and TrBACa.

device D), device C and device D still showed insignificant EQE roll-off of 7.2% and 3.9%, corresponding to η_r of 51.43% and 63.45%, which still exceed twice of the limit of 25% in a conventional fluorescent device.

2.5. "Hot Exciton" Channel of T-S Conversion

In addition to good injection and confinement of carrier charges in the emitting layer, there still is an essential internal factor to cause such high η_r and robust stability. First, the TTA mechanism does not play a role in achieving high η_s, because the brightness increases less than linearly at higher current density (Figure S3, Supporting Information).[39] We then performed PL decay measurements of pure NCBAOMe (TrBACa) and 1 wt% NCBAOMe (TrBACa):C545T films, all the films only exhibit prompt fluorescence emissions of short PL lifetimes in a few seconds without any delayed component observed (Figure S4, Supporting Information). In order to find out the mechanism that could effect the probability for generating singlet bound states, NTOs of the first ten singlet and triplet excitations were calculated based on CAM-B3LYP to describe the character of electronic transitions for singlet and triplet excited states. For the sake of simplicity and conciseness, we analyze the dominant NTO pairs' contributions and the related weights for the first several singlet and triplet excited states for the pictorial description in **Figure 7**. As shown in Figure 7, both S_1, S_2, T_1, and T_2 states of NCBAOMe and TrBACa exhibit a typical character of LE state, while high-lying S_3 states of NCBAOMe and TrBACa show an obvious feature of CT state. For high-lying triplet excited state, T_3 state of NCBAOMe corresponds to the pure LE state, while T_3 state of TrBACa and T_4 state of NCBAOMe display a strong CT character transition.

To illustrate exciton decay and conversion process in EL devices, the excited state energy diagrams of the first ten singlet and triplet excited states were described carefully (**Figure 8**a). In the excited state energy diagram of NCBAOMe, a small singlet–triplet energy splitting (ΔE_{ST} = 0.11 eV) between S_3 and T_4 was found due to the strong CT character of them. Moreover, a large energy gap of 0.95 eV was estimated between T_3 and T_2 states in NCBAOMe, which may greatly restrict internal conversion (IC) decay from T_3 to T_2 according to the energy-gap law.[23] Although a small energy gap was discovered between T_4 and T_3, T_3 still acts as an obstacle in the hot exciton channel $T_4 \rightarrow S_3$ (Figure 8b). While in the excited state energy diagram of TrBACa, two distinguished features should be paid attention to. First, a smaller singlet–triplet energy splitting (ΔE_{ST} = 0.07 eV) between S_3 and T_3 was demonstrated in theoretical calculation, which may significantly decrease energy barrier during hot exciton RISC. Second, a larger energy gap of 1.07 eV was calculated between T_3 and T_2 states in TrBACa, leading to more effective hindrance of IC decay. Based on the above two points, as shown in Figure 8b, more effective RISC channel ($T_3 \rightarrow S_3 \rightarrow S_1$) would form in TrBACa.

It is worth noting that the energy gaps between high-lying TICT singlet and triplet excited state of NCBAOMe and TrBACa were smaller than most of the HLCT molecules reported.[23–26] The singlet–triplet energy splitting ΔE_{ST} is twice the value of

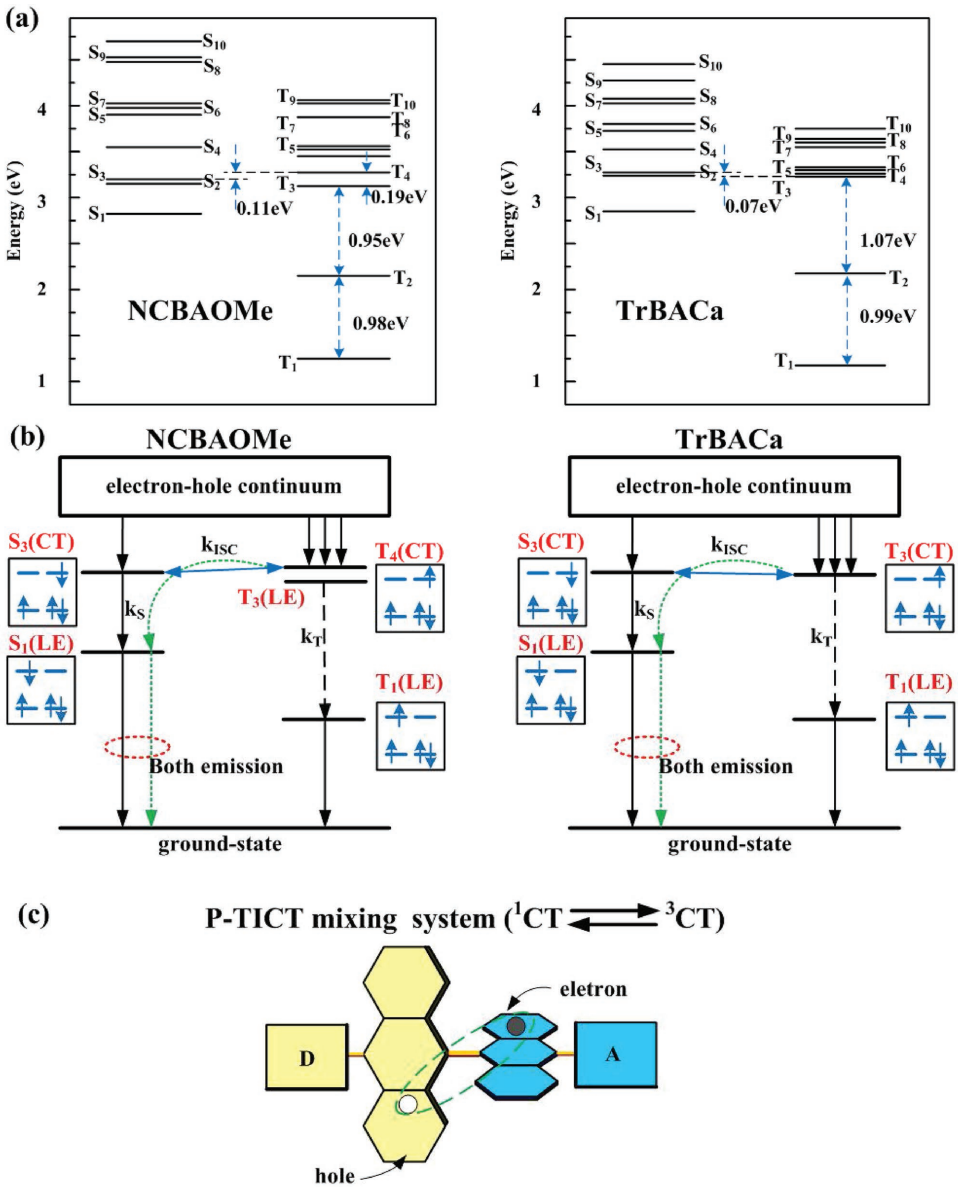

Figure 8. a) Excited state (singlet and triplet) energy diagram of NCBAOMe and TrBACa from TD-DFT/CAM-B3LYP calculations. b) Schematic of the exciton decay process in NCBAOMe and TrBACa devices. c) Schematic description of high-lying TICT intersystem crossing mechanism.

the electron-exchange integral J (ϕ, ϕ^*), which is proportional to the orbital overlap between ϕ and ϕ^*.[16] Therefore, smaller overlap in wavefunctions of electron and hole would lead to the smaller ΔE_{ST}. In the EL process, the electron and hole initially reside on acceptor and donor section, respectively, to form perpendicular TICT intermediate state (the precursors of lowest LE excitons) due to the almost perpendicular configuration of BA core, and the initial proportion of high-lying singlet and triplet TICT states follows spin statistics. As a result of highly twisted structure and effective separation of electron and hole, binding energy of the higher excited TICT intermediate state is very weak.[3] For limited overlap of electron–hole wave functions, singlet–triplet energy splitting of TICT intermediate state is very small, thus triplet-to-singlet high-lying TICT excited state transition (e.g., $T_3 \rightarrow S_3$ in TrBACa) would happen via the RISC process.[40–42] Besides, the high-lying TICT state is a spin–orbit, charge-transfer intersystem crossing mechanism (Figure 8c), which is especially enhanced in perpendicular torsional angle between twisted π system.[43,44] Since singlet exciton shows smaller binding energy (higher in energy) relative to triplet exciton, the direct relaxation from singlet TICT excited state to singlet exciton should be more faster due to larger overlaps in the singlet channel.[45] High-lying singlet and triplet TICT intermediate excited states are likely to be in intersystem crossing quasiequilibrium, from which the singlet bound exciton formation is more efficient,[46,47] the occurrence of such a mechanism could lead to significant high η_r and breakthrough of the 25% limit, and the η_r of C545T-doped device is lower than the nondoped device due to directly carrier trapping of C545T dopant. Particularly, triplet-to-singlet transition will achieve in

high-lying TICT excited state, thus serious efficiency roll-off due to accumulation of lowest triplet excited excitons would be avoided. Coupled with good injection and balanced transport property of carrier charges, robust efficiency stability at high current density can be realized.

3. Conclusion

In summary, we report two luminescent molecules NCBAOMe and TrBACa with a highly twisted donor–bianthracene–acceptor structure. From the theoretical computation and photophysical properties, we have demonstrated that NCBAOMe and TrBACa have obvious high-lying TICT characters and nearly LE-emission features in films. By using TrBACa as emitter in a non-doped device, high η_r of 70.5% and slightly efficiency roll-off of 10.5% at a high current density of 100 mA cm^{-2} (5307 cd m^{-2}) are obtained. Particularly, as a host material doped with fluorescent dopant C545T, the TrBACa-based device exhibits high η_r of 64.82% and negligible efficiency roll-off of only 0.9% at a high current density of 100 mA cm^{-2} (23615 cd m^{-2}). Our results provide a novel strategy to construct the highly efficient fluorescent OLED with high exciton utilization and robust stability at high current densities by using high-lying TICT intermediate excited states.

4. Experimental Section

General: The manipulation involving air-sensitive reagents was performed under an inert atmosphere of dry nitrogen. All the chemicals purchased were used without further purification unless otherwise stated. PL and absorption spectra were recorded by a Horiba Jobin Yvon Fluoromax-4 spectrophotometer and a Hitachi UV 3010 spectrophotometer, respectively. To measure the fluorescence quantum yields (Φ_f), degassed solutions of the compounds in CH_2Cl_2 were prepared. The concentration was adjusted so that the absorbance of the solution would be lower than 0.1. The excitation was performed at 380 nm, and quinine sulfate in 1.0 M H_2SO_4 solution, which has $\Phi_f = 0.56$, was used as a standard. The difference between the refractive index of the solvent and that of the standard should also be counted. The absolute PL quantum yields of films were measured using an integrating sphere excited at 379 nm with an absolute PL quantum yield measurement system (Hamamatsu C11347). Glass transition temperatures (T_g) were determined with a differential scanning calorimeter (DSC, TA instruments DSC200PC) at a heating rate of 10 °C min^{-1} under a nitrogen atmosphere. Cyclic voltammetry (CV) was performed using a Princeton Applied Research model 273 A potentiostat at a scan rate of 100 mV s^{-1}. All experiments were carried out in a three-electrode compartment cell with a Pt-sheet counter electrode, a glassy carbon working electrode and a Pt-wire reference electrode. The supporting electrolyte used was 0.1 M tetrabutylammonium perchlorate ($[Bu_4N]ClO_4$) solution in dry CH_2Cl_2 under a nitrogen atmosphere using ferrocene as an internal standard.

Device Fabrication and Testing: OLEDs were fabricated by thermal evaporation onto a cleaned glass substrate precoated with transparent and conductive ITO. Prior to organic layer deposition, ITO substrates were exposed to a UV–ozone flux for 10 min, following degreasing in acetone and isopropyl alcohol. All of the organic materials were purified by temperature-gradient sublimation in a vacuum. The devices were fabricated by conventional vacuum deposition of the organic layers, MoO_3, LiF, and Al cathode onto an ITO-coated glass substrate under a base pressure lower than 1×10^{-3} Pa. The thickness of each layer was determined by a quartz thickness monitor. The current density–voltage–luminance (*J–V–L*) characteristics of devices were measured with a Keithley 2602 and Source Meter. All measurements were carried out at room temperature under ambient conditions.

Computational Details: All the DFT calculations were carried out under Gaussian 09 (version D.01) package.[48] The ground state geometry was optimized using a long-range-correction DFT calculation with CAM-B3LYP hybrid functional[49] at the basis set level of 6-31G(d,p). The excited state geometry was optimized by TD-DFT[50] with the CAM-B3LYP being functional at the same basis set level. Based on the optimized configuration of ground state, the energy landscape of singlet and triplet states was evaluated using TD-CAM-B3LYP/6-31G(d,p). In order to examine the nature of the electronic transitions, NTOs[51] of absorption were evaluated for the excited states, involving both singlet and triplet states under TD-CAM-B3LYP/6-31G(d,p) using the geometry of ground state. Compositions of molecular orbits were analyzed using the GaussView 5.0 program.

Materials: See the details in the Supporting Information.

Supporting Information

Supporting Information is available from the Wiley Online Library or from the author.

Acknowledgements

Y.Y. and L.M. contributed equally to this work. This work was financially supported by the National Key R&D Program of China (Grant No. 2016YFB0400702) and the Fundamental Research Funds for the Central Universities.

Conflict of Interest

The authors declare no conflict of interest.

Keywords

charge transfer, efficiency roll-off, electroluminescence, fluorescent materials, hot excitons, radiative exciton production

Received: January 16, 2018
Revised: April 28, 2018
Published online: May 31, 2018

[1] C. W. Tang, S. A. VanSlyke, *Appl. Phys. Lett.* **1987**, *51*, 913.
[2] C. Adachi, M. A. Baldo, S. R. Forrest, M. E. Thompson, *J. Appl. Phys.* **1999**, *11*, 285.
[3] M. Segal, M. Singh, K. Rivoire, S. Difley, T. Van Voorhis, M. A. Baldo, *Nat. Mater.* **2007**, *6*, 374.
[4] L. S. Hung, C. H. Chen, *Mater. Sci. Eng. R* **2002**, *39*, 143.
[5] S. R. Forrest, *Nature* **2004**, *428*, 911.
[6] Y. Sun, N. C. Giebink, H. Kanno, B. Ma, M. E. Thompson, S. R. Forrest, *Nature* **2006**, *440*, 908.
[7] S. Reineke, F. Lindner, G. Schwartz, N. Seidler, K. Walzer, B. Sussem, K. Leo, *Nature* **2009**, *459*, 234.

[8] P. W. Atkins, *Molecular Quantum Mechanics*, Oxford University Press, New York **1983**.
[9] M. A. Baldo, D. F. O'Brien, M. E. Thompson, S. R. Forrest, *Phys. Rev. B* **1999**, *60*, 14422.
[10] M. A. Baldo, D. F. O'brien, Y. You, A. Shoustikov, S. Sibley, M. E. Thompson, S. R. Forrest, *Nature* **1998**, *395*, 151.
[11] Y. G. Ma, H. Y. Zhang, J. C. Shen, C. M. Chen, *Synth. Met.* **1998**, *94*, 245.
[12] C. Adachi, M. A. Baldo, M. E. Thompson, S. R. Forrest, *J. Appl. Phys.* **2001**, *90*, 5048.
[13] K. H. Kim, C. K. Moon, J. H. Lee, S. Y. Kim, J. J. Kim, *Adv. Mater.* **2014**, *26*, 3844.
[14] K. Udagawa, H. Sasabe, C. Cai, J. Kido, *Adv. Mater.* **2014**, *26*, 5062.
[15] S. Reineke, K. Walzer, K. Leo, *Phys. Rev. B* **2007**, *75*, 125328.
[16] A. Endo, M. Ogasawara, A. Takahashi, D. Yokoyama, Y. Kato, C. Adachi, *Adv. Mater.* **2009**, *21*, 4802.
[17] H. Uoyama, K. Goushi, K. Shizu, H. Nomura, C. Adachi, *Nature* **2012**, *492*, 234.
[18] S. Hirata, Y. Sakai, K. Masui, H. Tanaka, S. Y. Lee, H. Nomura, N. Nakamura, M. Yasumatsu, H. Nakanotani, Q. Zhang, K. Shizu, H. Miyazaki, C. Adachi, *Nat. Mater.* **2015**, *14*, 330.
[19] D. Zhang, L. Duan, C. Li, Y. Li, H. Li, D. Zhang, Y. Qiu, *Adv. Mater.* **2014**, *26*, 5050.
[20] X. K. Liu, Z. Chen, C. J. Zheng, M. Chen, W. Liu, X. H. Zhang, C. S. Lee, *Adv. Mater.* **2015**, *27*, 2025.
[21] T. Komino, H. Nomura, T. Koyanagi, C. Adachi, *Chem. Mater.* **2013**, *25*, 3038.
[22] K. Masui, H. Nakanotani, C. Adachi, *Org. Electron.* **2013**, *14*, 2721.
[23] W. Li, Y. Pan, R. Xiao, Q. Peng, S. Zhang, D. Ma, F. Li, F. Shen, Y. Wang, B. Yang, Y. Ma, *Adv. Funct. Mater.* **2014**, *24*, 1609.
[24] S. Zhang, L. Yao, Q. Peng, W. Li, Y. Pan, R. Xiao, Y. Gao, C. Gu, Z. Wang, P. Lu, F. Li, S. Su, B. Yang, Y. Ma, *Adv. Funct. Mater.* **2015**, *25*, 1755.
[25] L. Yao, S. Zhang, R. Wang, W. Li, F. Shen, B. Yang, Y. Ma, *Angew. Chem., Int. Ed.* **2014**, *53*, 2119.
[26] C. Wang, X. Li, Y. Pan, S. Zhang, L. Yao, Q. Bai, W. Li, P. Lu, B. Yang, S. Su, Y. Ma, *Appl. Mater. Interfaces* **2016**, *8*, 3041.
[27] Y. Yu, Z. Wu, Z. Li, B. Jiao, L. Li, L. Ma, D. Wang, G. Zhou, X. Hou, *J. Mater. Chem. C* **2013**, *1*, 8117.
[28] Y. Yu, B. Jiao, Z. Wu, Z. Li, L. Ma, G. Zhou, W. Yu, S. K. So, X. Hou, *J. Mater. Chem. C* **2014**, *2*, 9375.
[29] P. Zhang, W. Dou, Z. Ju, L. Yang, X. Tang, W. Liu, Y. Wu, *Org. Electron.* **2013**, *14*, 915.
[30] N. Asami, T. Takaya, S. Yabumoto, S. Shigeto, H. Hamaguchi, K. Iwata, *J. Phys. Chem. A* **2010**, *114*, 6351.
[31] F. C. Grozema, M. Swart, R. W. J. Zijlstra, J. J. Piet, L. D. A. Siebbeles, P. T. V. Duijnen, *J. Am. Chem. Soc.* **2005**, *127*, 11019.
[32] F. Bell, D. H. Waring, *J. Chem. Soc.* **1949**, *0*, 267.
[33] U. Müller, M. Baumgarten, *J. Am. Chem. Soc.* **1995**, *117*, 5840.
[34] Z. R. Grabowski, K. Rotkiewicz, W. Rettig, *Chem. Rev.* **2003**, *103*, 3899.
[35] J. Catalan, C. Diaz, V. Lopez, P. Perez, R. M. Claramunt, *J. Phys. Chem.* **1996**, *100*, 18392.
[36] B. Peng, S. Xu, Z. Chi, J. Xu, *Prog. Chem.* **2013**, *25*, 1805.
[37] M. A. Baldo, S. R. Forrest, *Phys. Rev. B* **2000**, *62*, 10958.
[38] D. Y. Kondakov, *J. Appl. Phys.* **2007**, *102*, 114504.
[39] C. Ganzorig, M. Fujihira, *Appl. Phys. Lett.* **2002**, *81*, 3137.
[40] S. Difley, D. Beljonne, T. V. Voorhis, *J. Am. Chem. Soc.* **2008**, *130*, 3420.
[41] A. Kadashchuk, A. Vakhnin, I. Blonski, D. Beljonne, Z. Shuai, J. L. Brédas, V. I. Arkhipov, P. Heremans, E. V. Emelianova, H. Bässler, *Phys. Rev. Lett.* **2000**, *93*, 066803.
[42] V. Jankus, M. Audemir, F. B. Dias, A. P. Monkman, *Adv. Sci.* **2016**, *3*, 1500221.
[43] Z. E. X. Dance, S. M. Mickley, T. M. Wilson, A. B. Ricks, A. M. Scott, M. A. Ratner, M. R. Wasielewski, *J. Phys. Chem. A* **2008**, *112*, 4194.
[44] H. van Willigen, G. Jones II, M. S. Farahat, *J. Phys. Chem.* **1996**, *100*, 3312.
[45] K. Tandon, S. Ramasesha, S. Mazumdar, *Phys. Rev. B* **2003**, *67*, 045109.
[46] S. Karabunarliev, E. R. Bittner, *Phys. Rev. Lett.* **2003**, *90*, 057402.
[47] S. Karabunarliev, E. R. Bittner, *J. Chem. Phys.* **2003**, *119*, 3988.
[48] M. J. Frisch, G. W. Trucks, H. B. Schlegel, G. E. Scuseria, M. A. Robb, J. R. Cheeseman, G. Scalmani, V. Barone, B. Mennucci, G. A. Petersson, H. Nakatsuji, M. Caricato, X. Li, H. P. Hratchian, A. F. Izmaylov, J. Bloino, G. Zheng, J. L. Sonnenberg, M. Hada, M. Ehara, K. Toyota, R. Fukuda, J. Hasegawa, M. Ishida, T. Nakajima, Y. Honda, O. Kitao, H. Nakai, T. Vreven, J. A. Montgomery Jr., J. E. Peralta, F. Ogliaro, M. Bearpark, J. J. Heyd, E. Brothers, K. N. Kudin, V. N. Staroverov, R. Kobayashi, J. Normand, K. Raghavachari, A. Rendell, J. C. Burant, S. S. Iyengar, J. Tomasi, M. Cossi, N. Rega, J. M. Millam, M. Klene, J. E. Knox, J. B. Cross, V. Bakken, C. Adamo, J. Jaramillo, R. Gomperts, R. E. Stratmann, O. Yazyev, A. J. Austin, R. Cammi, C. Pomelli, J. W. Ochterski, R. L. Martin, K. Morokuma, V. G. Zakrzewski, G. A. Voth, P. Salvador, J. J. Dannenberg, S. Dapprich, A. D. Daniels, Ö. Farkas, J. B. Foresman, J. V. Ortiz, J. Cioslowski, D. J. Fox, *Gaussian 09, Revision D.01*, Gaussian, Wallingford, CT **2009**.
[49] T. Yanai, D. P. Tew, N. C. Handy, *Chem. Phys. Lett.* **2004**, *393*, 51.
[50] E. Runge, E. K. U. Gross, *Phys. Rev. Lett.* **1984**, *52*, 997.
[51] R. L. Martin, *J. Chem. Phys.* **2003**, *118*, 4775.